ISSN 2176-5480

22nd International Congress of Mechanical Engineering (COBEM 2013)
November 3-7, 2013, Ribeirão Preto, SP, Brazil

3D COMPOSITIONAL RESERVOIR SIMULATION USING UNSTRUCTURED GRIDS IN HOMOGENEOUS RESERVOIRS

André Luiz de Souza Araujo
Federal Institute of Education, Science and Technology of Ceará, Fortaleza, Ceará, Brazil.
andre@ifce.edu.br

Bruno Ramon Batista Fernandes
Federal University of Ceará, Laboratory of Computation Fluid Dynamics, LDFC, Fortaleza, Ceará, Brazil.
brbfernandes@ldfc.ufc.br

Robson Melo Araujo
Federal University of Ceará, Laboratory of Computation Fluid Dynamics, LDFC, Fortaleza, Ceará, Brazil.
robson@ldfc.ufc.br

Edilson Pimentel Drumond Filho
Federal University of Ceará, Laboratory of Computation Fluid Dynamics, LDFC, Fortaleza, Ceará, Brazil.
edilson@ldfc.ufc.br

Ivens da Costa Menezes Lima
Federal University of Ceará, Laboratory of Computation Fluid Dynamics, LDFC, Fortaleza, Ceará, Brazil.
ivenscml@ldfc.ufc.br

Francisco Marcondes
Federal University of Ceará, Department of Mettalurgical Engineering and Material Science, Fortaleza, Ceará, Brazil.
marcondes@ufc.br

Kamy Sepehrnoori
The University of Texas at Austin, Department of Petroleum and Geosystems Engineering, 200 E. Dean Keeton St., C0300, Austin, TX 78712-1585.
kamys@mail.utexas.edu

Abstract. *This paper presents a 3D implementation of an element-based finite-volume method (EbFVM) using hexahedron, tetrahedron, prism and pyramid elements in conjunction with a compositional reservoir simulator. The EbFVM approach combines the conservative advantage of the finite volume method and adds flexibility to handle irregular geometries. The EbFVM is implemented into the UTCOMP simulator considering a full permeability tensor formulation for the advection terms. The UTCOMP simulator was developed at the Center for Petroleum and Geosystems Engineering at The University of Texas at Austin for the simulation of enhanced recovery processes. UTCOMP is a compositional multiphase/multi-component, Implicit Pressure Explicit Composition simulator (IMPEC), which can handle the simulation of miscible gas flooding processes. Only permeability and porosity are stored into the cells, and all other properties are evaluated in the grid vertex, and therefore the balance equations are performed in a cell-vertex approach. The balance equations are locally evaluated into the elements and each piece of the elements, called sub-control volume, are assembled to form the control volumes around each vertices. The results of several cases studies are presented in terms of volumetric rates of oil and gas, and saturation fields. The results of the original formulation of the UTCOMP simulator using Cartesian meshes are also presented.*

Keywords: *EbFVM, Unstructured Meshes, Compositional Reservoir Simulation, UTCOMP simulator*

1. INTRODUCTION

One of the key issues in petroleum reservoir simulation is the correct representation of the irregular reservoir shape. Most of simulators are based on Cartesian grids. However, Cartesian grid does not present the necessary flexibility for modeling the complex shapes of reservoirs commonly found in fields. Boundary fitted coordinates and unstructured grids are much more flexible options to model irregular shapes of reservoirs (Marcondes *et al*., 2008; Marcondes and Sepehrnoori, 2007, 2010; Marcondes *et al*., 2013). This paper is devoted to the application of 3D unstructured meshes. Application of unstructured meshes on petroleum reservoir simulation started with the works of Forsyth (1990), Fung *et. al.* (1991), and Gottardi and Dall'Ollio (1992). The aforementioned authors uses linear triangle elements for the 2D discretization of material balance equations. The numerical approximation equations were first obtained for single phase flows, and the transmissibilities were multiplied by mobilities in order to obtain the equation to multiphase flows. This approach was first called Control Volume Finite Element Method (CVFEM). Later on, Edwards (2002a, 2002b)

ISSN 2176-5480

presented the multipoint-flux approximation. This technique is defined by the storage of all physical properties at the vertex of the elements of the grid, including the porosity and the absolute permeability tensor, and it was developed for 2D discretization using triangular and quadrilateral elements.

Cordazzo (2004) and Cordazzo *et. al.* (2004a-b), based on the works of Raw (1985) and Baliga and Patankar (1983) developed a method to solve water flooding problems. The approach is similar to the CVFEM technique concerning the final approximate equations, although this new method derives the equations directly from the multiphase/multi-component flow assumption, since, is shown by these authors that the multiplication of the single-phase flow equations by the phase mobilities does not adequately approximates the equations for multiphase flow. This new scheme was called Element-based Finite Volume Method (EbFVM), a more suitable denomination for a technique that adds the idea of elements and shape functions from the finite element method to a simple finite volume method. Excellent results were obtained and little grid orientation effects were observed, for an implicit pressure explicit saturation (IMPES) formulation. Later, Paluszny *et. al.* (2007) presented a fully 3D discretization for hexahedron, tetrahedron, prism and pyramids elements in conjunction with water flooding problems. More recently, Marcondes et al. (2013) presented a 3D discretization using the EbFM formulation for a simulation of composional reservoir simulation in conjunction with a fully implicit approach.

In this work, the EbFVM method is investigated with homogeneous 3D reservoir using four kind of elements: hexahedron, tetrahedron, prism, and pyramid. Each element has a constant porosity and permeability tensor, but the values of these properties are not necessarily the same between different elements. Except for these two properties, the rest of the physical properties are evaluated at the vertices of each element, giving rise to a cell vertex approach. The technique was implemented on the UTCOMP simulator, developed at the Center of Petroleum and Geosystems Engineering at The University of Texas at Austin for the simulation of enhanced recovery oil processes. UTCOMP is a compositional multiphase/multi-component, Implicit Pressure Explicit Composition (IMPEC) simulator, capable of handling miscible gas flooding processes. Three case studies were investigated using regular and irregularly shaped reservoirs with different number of hydrocarbon components applying all four-element types. Comparison of the results obtained for the regular reservoir show a reasonable accuracy for all four elements and a good agreement when comparing the results with the Cartesian grid formulation. Also, accurate results were obtained when simulating a case study involving irregularly shaped reservoir.

2. GOVERNING EQUATIONS

According to Wang *et. al.* (1997), three equations are required in order to describe an isothermal, multi-component, multiphase flow in a porous medium: the material balance equation for all components, phase equilibrium equation and the equation for constraining phase saturations and component concentrations.

Considering a full symmetric permeability tensor, the material balance equation for each of the *i-th* components is written as follows:

$$\frac{\partial N_i}{\partial t} - \nabla \cdot \left[-\sum_{j=1}^{n_p} \xi_j \lambda_j x_{ij} \vec{\vec{k}} \cdot \vec{\nabla} \Phi_j - \phi \xi_j S_j \vec{\vec{K}}_{ij} \cdot \vec{\nabla} x_{ij} \right] - \frac{q_i}{V_b} = 0 \ ; \ i = w, 1, 2, \cdots, n_c \,, \tag{1}$$

where n_{c+1} represents the total number of components (hydrocarbon components + water), n_p denotes the number of phases, ϕ is the reservoir porosity, ξ_j and λ_j are the molar density and relative mobility of each of the *j-th* phase, respectively, N_i is the number of moles of the *i-th* component per unit of pore volume, x_{ij} is the molar fraction of the *i-th* component in the *j-th* phase, V_b is the volume of a control-volume that could contain a well, and $\vec{\vec{K}}$ is the absolute permeability tensor.

The potential of the *j-th* phase (Φ_j) is given by

$$\Phi_j = P_j - \gamma_j D \,. \tag{2}$$

In Eq. (2), P_j is the pressure of the *j-th* phase and D is the reservoir depth, evaluated as positive in the downward direction. The first partial derivative of the total Gibbs free energy for the independent variables results on the equality of component fugacities in all phases.

$$\begin{aligned} f_i^g - f_i^o = 0 \ \ ; \ \ i = 1, \ldots, n_c \\ f_i^{L_2} - f_i^o = 0 \ \ ; \ \ i = 1, \ldots, n_c \end{aligned} \,. \tag{3}$$

ISSN 2176-5480

In Eq. (3), L_2 denotes the second liquid phase and n_c is the number of hydrocarbon components, the fugacity of component i in phase j is given by, $f_i^{\,j} = \ln\left(x_{ij}\,\phi_{ij}\right)$, where ϕ_{ij} is the fugacity coefficient of component i in the *j-th* phase. Using the molar fraction restriction the solution for Eq. (3) is given.

$$\sum_{i=1}^{n_c} x_{ij} - 1 = 0\ ,\ j = 2,..,n_p \quad ; \quad \sum_{i=1}^{n_c} \frac{z_i\,(K_i - 1)}{1 + \nu\,(K_i - 1)} = 0\ , \tag{4}$$

where K_i is the equilibrium ratio for the *i-th* component, z_i represents the overall molar fraction of the *i-th* component and ν is the mole fraction of the gas phase in the absence of water.

The volume constraint considers that the pore volume of every cell has to be filled by all phases present in the reservoir which is given by

$$V_b \sum_{i=1}^{n_c+1} \left(\phi\, N_i\right) \sum_{j=1}^{n_p} L_j\, \overline{v}_j - V_p = 0\,, \tag{5}$$

where V_p denotes the pore volume, $\overline{v}_j$ and L_j are the molar volume of and the amount of the *j-th* phase, respectively.

3. APPROXIMATE EQUATION

In the EbFVM method each element is divided into sub-elements, also called sub-control volumes. All sub-control volumes that share the same vertex are then assembled to build the control volume around each vertex. For this approach, the material balance, Eq. (1), is first integrated for every one of the sub-control volumes of each element. Then, the final equation of each sub-control volume is built getting contributions from all sub-control volumes that shares each vertex. The division of the elements in sub-control volumes is performed according the number of vertices of each element. Fig. 1 presents the sub-control volumes and the integration surfaces for each one of the aforementioned elements.

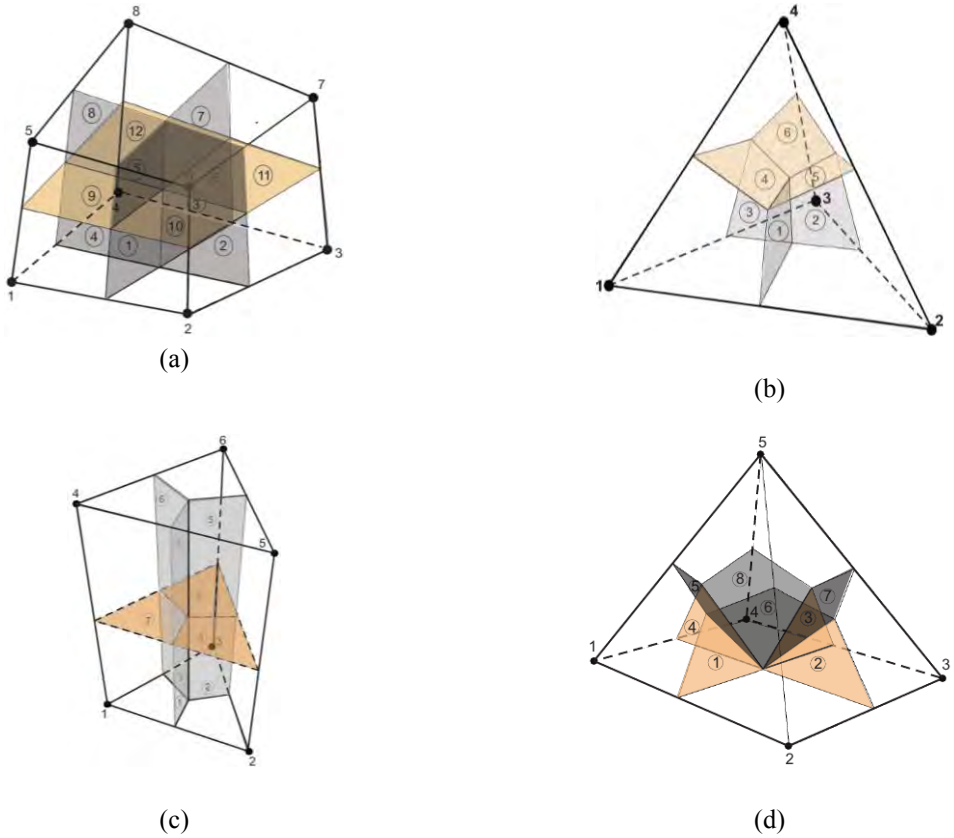

(a) (b) (c) (d)

Figure 1. Sub-control volumes for the four elements types: (a) hexahedron, (b) tetrahedron, (c) prism and (d) pyramid.

ISSN 2176-5480

As we can see in Fig. 1, except for the pyramid type, each sub-control volume has three integration surfaces associated which are quadrilateral. The pyramid elements present a singular case, since there are actually two types of sub-control volumes, the ones associated with the base, with two triangular integration surfaces and only one quadrilateral integration surface, and the one associated with the apex, with four quadrilateral integrations surfaces.

The integration of Eq. (1) for each sub control-volume followed by the application of the Gauss theorem for the advective term gives:

$$\int_V \frac{\partial(\phi N_i)}{\partial t} dV - \int_A \sum_{j=1}^{n_p} \xi_j \, x_{ij} \, \lambda_j \overline{\overline{K}} \cdot \nabla \Phi_j \cdot \overrightarrow{dA} - \int_V \frac{q_i}{V_b} = 0 \; ; \; i = 1, 2, .., n_{c+1} \tag{6}$$

In order to evaluate the first term of Eq. (6), first the shape functions need to be defined for each element typr. The shape functions for hexahedron, tetrahedron, prism and pyramids elements, are respectively given by

$$\begin{aligned} N_1(s,t,p) &= \frac{(1+s)*(1-t)*(1+p)}{8} \; ; N_2(s,t,p) = \frac{(1+s)*(1-t)*(1-p)}{8} \\ N_3(s,t,p) &= \frac{(1-s)*(1-t)*(1-p)}{8} \; ; N_4(s,t,p) = \frac{(1-s)*(1-t)*(1+p)}{8} \\ N_5(s,t,p) &= \frac{(1+s)*(1+t)*(1+p)}{8} \; ; N_6(s,t,p) = \frac{(1+s)*(1+t)*(1-p)}{8} \\ N_7(s,t,p) &= \frac{(1-s)*(1+t)*(1-p)}{8} \; ; N_8(s,t,p) = \frac{(1-s)*(1+t)*(1+p)}{8} \end{aligned}, \tag{7}$$

$$\begin{aligned} N_1(s,t,p) &= 1-s-t-p \quad ; \quad N_2(s,t,p) = s \\ N_3(s,t,p) &= t \quad ; \quad N_4(s,t,p) = p \end{aligned}, \tag{8}$$

$$\begin{aligned} N_1(s,t,p) &= (1-s-t)*(1-p) \quad ; \quad N_2(s,t,p) = s*(1-p) \\ N_3(s,t,p) &= t*(1-p) \quad ; \quad N_4(s,t,p) = p*(1-s-t) \\ N_5(s,t,p) &= s*p \quad ; \quad N_6(s,t,p) = t*p \end{aligned}, \tag{9}$$

$$\begin{aligned} N_1(s,t,p) &= \frac{1}{4}[(1-s)(1-t) - p + s*t*p/(1-p)] \\ N_2(s,t,p) &= \frac{1}{4}[(1+s)(1-t) - p - s*t*p/(1-p)] \\ N_3(s,t,p) &= \frac{1}{4}[(1+s)(1+t) - p - s*t*p/(1-p)] \\ N_4(s,t,p) &= [(1-s)(1+t) - p - s*t*p/(1-p)] \\ N_5(s,t,p) &= p \end{aligned}. \tag{10}$$

In Eq. (7) through Eq. (10), *s*, *t* and *p* represent the local axis in the transformed domain. Throughout shape functions, any geometrical or physical properties can be evaluated inside elements

$$x(s,t,p) = \sum_{i=1}^{Nv} N_i \, x_i \; ; \; y(s,t,p) = \sum_{i=1}^{Nv} N_i \, y_i \; ; \; z(s,t,p) = \sum_{i=1}^{Nv} N_i \, z_i \; ; \; \Phi_j(s,t,p) = \sum_{i=1}^{Nv} N_i \, \Phi_{ji} \; . \tag{11}$$

In Eq. (11), N_v and N_i are, respectively, the number of vertex and the shape functions of each element The gradient phase potential are given by

$$\frac{\partial \Phi_j}{\partial x} = \sum_{i=1}^{Nv} \frac{\partial N_i}{\partial x} \Phi_{ji} \quad ; \quad \frac{\partial \Phi_j}{\partial y} = \sum_{i=1}^{Nv} \frac{\partial N_i}{\partial y} \Phi_{ji} \; ; \; \frac{\partial \Phi_j}{\partial z} = \sum_{i=1}^{Nv} \frac{\partial N_i}{\partial z} \Phi_{ji} \; . \tag{12}$$

However, these gradients can only be fully evaluated when the derivatives of the shape functions related to x, y and z axis are computed. The derivatives are presented in Eq. (13). Further details can be found in Hurtado (2011) and Marcondes *et al.* (2013).

ISSN 2176-5480

$$\begin{aligned}
\frac{\partial N_i}{\partial x} &= \frac{1}{\det(J_t)}\left(\frac{\partial y}{\partial t}\frac{\partial z}{\partial p}-\frac{\partial y}{\partial p}\frac{\partial z}{\partial t}\right)\frac{\partial N_i}{\partial s}-\frac{1}{\det(J_t)}\left(\frac{\partial y}{\partial s}\frac{\partial z}{\partial p}-\frac{\partial y}{\partial p}\frac{\partial z}{\partial s}\right)\frac{\partial N_i}{\partial t}+\frac{1}{\det(J_t)}\left(\frac{\partial y}{\partial s}\frac{\partial z}{\partial t}-\frac{\partial y}{\partial t}\frac{\partial z}{\partial s}\right)\frac{\partial N_i}{\partial p} \\
\frac{\partial N_i}{\partial y} &= -\frac{1}{\det(J_t)}\left(\frac{\partial x}{\partial t}\frac{\partial z}{\partial p}-\frac{\partial x}{\partial p}\frac{\partial z}{\partial t}\right)\frac{\partial N_i}{\partial s}+\frac{1}{\det(J_t)}\left(\frac{\partial x}{\partial s}\frac{\partial z}{\partial p}-\frac{\partial x}{\partial p}\frac{\partial z}{\partial s}\right)\frac{\partial N_i}{\partial t}-\frac{1}{\det(J_t)}\left(\frac{\partial x}{\partial s}\frac{\partial z}{\partial t}-\frac{\partial x}{\partial t}\frac{\partial z}{\partial s}\right)\frac{\partial N_i}{\partial p} \\
\frac{\partial N_i}{\partial z} &= \frac{1}{\det(J_t)}\left(\frac{\partial x}{\partial t}\frac{\partial y}{\partial p}-\frac{\partial x}{\partial p}\frac{\partial y}{\partial t}\right)\frac{\partial N_i}{\partial s}-\frac{1}{\det(J_t)}\left(\frac{\partial x}{\partial s}\frac{\partial y}{\partial p}-\frac{\partial x}{\partial p}\frac{\partial y}{\partial s}\right)\frac{\partial N_i}{\partial t}+\frac{1}{\det(J_t)}\left(\frac{\partial x}{\partial s}\frac{\partial z}{\partial t}-\frac{\partial x}{\partial t}\frac{\partial y}{\partial s}\right)\frac{\partial N_i}{\partial p}
\end{aligned}, \tag{13}$$

where $det(J_t)$ is the Jacobian determinant of the transformation, which needs to be computed at the center of each sub-control volume, is given by the following equation:

$$\det(J_t)=\frac{\partial x}{\partial s}\left(\frac{\partial y}{\partial t}\frac{\partial z}{\partial p}-\frac{\partial y}{\partial p}\frac{\partial z}{\partial t}\right)-\frac{\partial x}{\partial t}\left(\frac{\partial y}{\partial s}\frac{\partial z}{\partial p}-\frac{\partial y}{\partial p}\frac{\partial z}{\partial s}\right)+\frac{\partial x}{\partial p}\left(\frac{\partial y}{\partial s}\frac{\partial z}{\partial t}-\frac{\partial y}{\partial t}\frac{\partial z}{\partial s}\right) \tag{14}$$

The definition of the volumes of each sub-control volume and the area of each interface is also required for the evaluation of integral term of Eq. (6). The volumes of each sub-control volume for hexahedron, tetrahedron, prism and pyramids are, in that order, given by:

$$Vscv_i=\det(J_t), \tag{15}$$

$$Vscv_i=\det(J_t)/6, \tag{16}$$

$$Vscv_i=\det(J_t)/12, \tag{17}$$

$$Vscv_i=\begin{cases}2*\det(J_t)/9 & for \quad i=1,...,4\ (base)\\ 4*\det(J_t)/9 & for \quad i=5\ (apex)\end{cases}. \tag{18}$$

The area of each interface for a hexahedron element follows.

$$\begin{aligned}
d\vec{A}=&\left(\frac{\partial y}{\partial m}\frac{\partial z}{\partial n}-\frac{\partial y}{\partial n}\frac{\partial z}{\partial m}\right)dm\,dn\,\vec{i}-\left(\frac{\partial x}{\partial n}\frac{\partial z}{\partial m}-\frac{\partial x}{\partial m}\frac{\partial z}{\partial n}\right)dm\,dn\,\vec{j}+\\
&\left(\frac{\partial x}{\partial m}\frac{\partial y}{\partial n}-\frac{\partial x}{\partial n}\frac{\partial y}{\partial m}\right)dm\,dn\,\vec{k}
\end{aligned}. \tag{19}$$

In Eq. (19), *m* and *n* represent the local system *s*, *t* or *p*. The evaluation of the area for each interface for the other types of elements is similar.

Now the accumulation term can be properly expressed through Eq. (15) to Eq. (18), and the advective flux by Eq. (19) and the equivalent equations for other elements and evaluating the physical properties through an explicit approach the following expressions for the accumulation term (*Acc*) and advective flux (*F*) are obtained:

$$Acc_{m,i}=Vscv_{m,i}\left(\left(\frac{\phi N_m}{\Delta t}\right)_i^{n+1}-\left(\frac{\phi N_m}{\Delta t}\right)_i^{n}\right) \quad ; \quad m=1,N_v, \tag{20}$$

$$\begin{aligned}
F_{m,i} &= \int_A \sum_{j=1}^{n_p}(\xi_j\, x_{ij}\, \lambda_j \overline{\overline{K}}\cdot\vec{\nabla}\Phi_j+\phi\xi_j S_j \vec{\vec{K}}_{ij}\cdot\vec{\nabla}x_{ij})\cdot\overrightarrow{dA} \\
&= \int_A \sum_{j=1}^{n_p}\left(\xi_j\, x_{ij}\, \lambda_j k_{lp}\right)^n\left(\frac{\partial\Phi_j}{\partial x_p}\right)^{n+1} dA_l+\int_A \sum_{j=1}^{n_p}\left(\phi\xi_j\, S_j\, k_{ij,lp}\frac{\partial x_{ij}}{\partial x_p}\right)^n dA_l \quad ; \quad .
\end{aligned} \tag{21}$$

$i=1,n_c+1$; $m=1,N_v$; $l,p=1,2$

ISSN 2176-5480

The superscripts ′n+1′ and ′n′ in the Eqs. (22) and (23) means properties evaluated in the current and the previous time-step, respectively. The analysis of Eq. (21) shows the necessity of computing molar densities, molar fractions and mobilities for the interfaces of each sub-control volume. An upwind scheme was applied in order to evaluate these properties. Considering, for instance, the integration point 1 in Fig. 1a, the mobility is given by

$$\begin{aligned} &\lambda_{j1} = \lambda_{j2} \quad if \quad \overline{\overline{K}}.\nabla\Phi_j.\overrightarrow{dA}\Big|_{ip1} \le 0 \\ &\lambda_{j1} = \lambda_{j1} \quad if \quad \overline{\overline{K}}.\nabla\Phi_j.\overrightarrow{dA}\Big|_{ip1} > 0 \end{aligned} \quad . \tag{22}$$

Inserting Eq. (20) and Eq. (21) into Eq. (6), the resulting equation is:

$$Acc_{m,i} + F_{m,i} + q_i = 0 \;\; ; \quad m = 1,...,N_v \; ; \; i = 1,...,n_c + 1 \, . \tag{23}$$

Eq. (23) represents the conservation balance for each sub-control volume of every element. The equation of each control volume around each vertex is obtained by summing up Eq. (23) for each sub-control volume that shares that vertex. A similar procedure needs to be performed to the pressure equation.

4. RESULTS

The results of three case studies using the EbFVM approach are presented in this section. The first case is a gas flooding simulation into a quarter of five-spot configuration, and the other two cases are related to a gas flooding in an irregular configuration. The first case is a high pressure reservoir with gas injection. The reservoir data, fluid composition data and binary coefficients values are given in Tabs. 1 through 3, respectively. In tables 2 and 3, the pseudo component NC16 denotes a lumped component that mimics a heavy hydrocarbon component.

Table 1. Reservoir data for case 1.

Property	Value	Unit
Width	170.688	m
Length	170.688	m
Thickness	30.480	m
Porosity	0.30	-
Water Initial Saturation	0.25	-
Initial Pressure	20.648	MPa
Permeability in X and Y	200	mD
Permeability in Z	20	mD
Formation Temperature	299.817	K
Producer Bottom Hole Pressure	20.648	MPa
Injector's Gas Rate	6.554E-03	m^3/s

Table 2. Fluid compositions for case 1.

Component	Initial Reservoir Composition	Injection Fluid Composition
CO_2	0.0100	0.9500
C1	0.0190	0.0500
NC16	0.8000	0.0000

Table 3. Binary interaction coefficients for case 2.

Component	CO_2	C1	NC16
CO_2	0.00	0.12	0.12
C1	0.12	0.00	0.00
NC16	0.12	0.00	0.00

Figures 2 and 3 present the oil and gas rates obtained with the all the four types of elements. The results obtained with a very refined Cartesian mesh are also shown.

ISSN 2176-5480

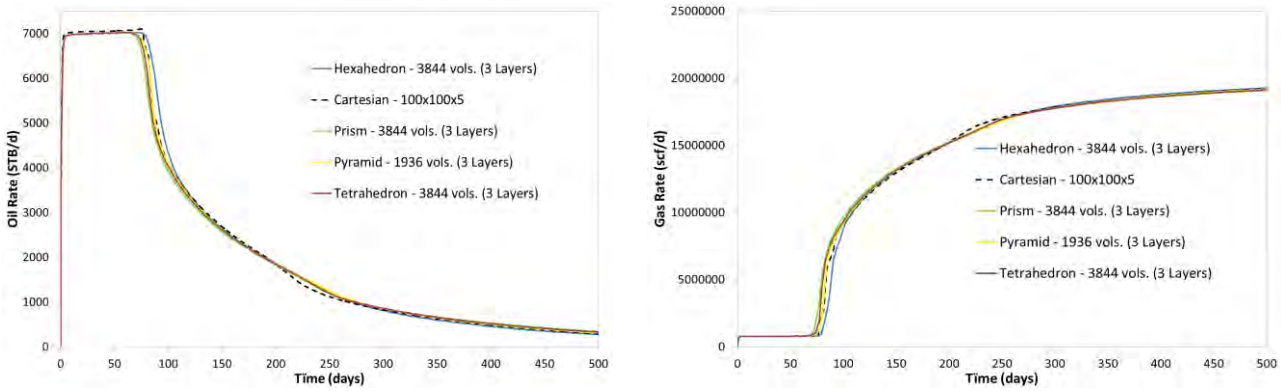

(a) (b)

Figure 2. Oil (a) and gas (a) rate for case 1.

From Figs. 2 and 3, it possible to conclude that the results obtained with the EbFVM formulation for all investigated elements presents a satisfactory match. The results are also in a good agreement with the results from Cartesian grid. It is also worth to mention the drastically higher level of refinement required for the Cartesian grid to achieve the same approximate solution of the EbFVM approach for all elements investigated. In this case study, only one hydrocarbon phase is formed, due to the high reservoir pressure and the fact that the binary coefficients were not considered. The oil saturation front at 500 days of simulation is presented in Figure 4. From this figure is possible to see that agreement between the four types of elements studied and the Cartesian mesh was obtained.

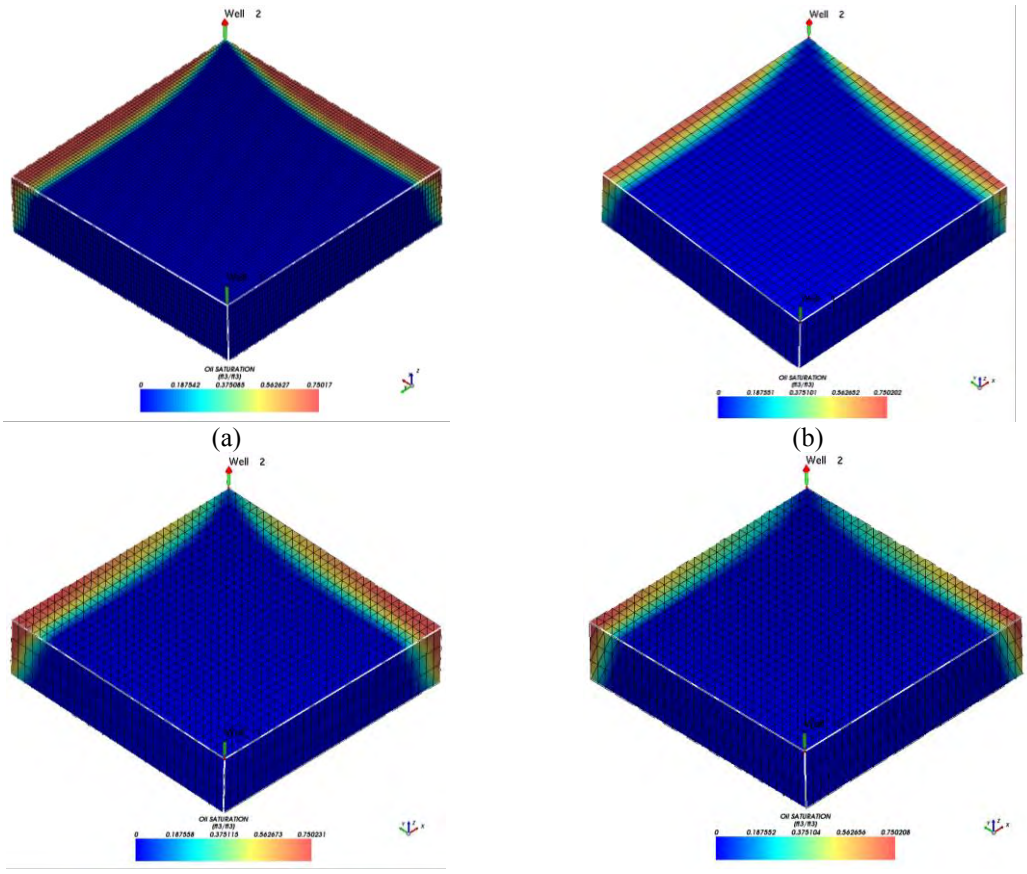

(a) (b)

(c) (d)

ISSN 2176-5480

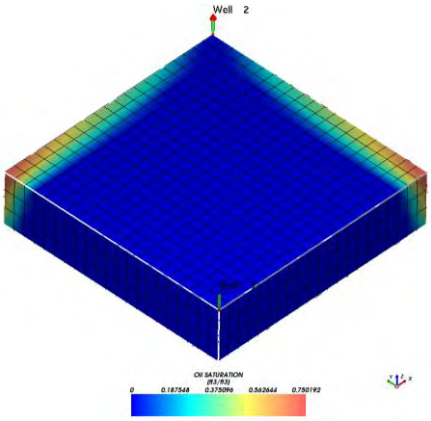

(e)

Figure 3. Oil saturation at 500 days for case 1. (a) Cartesian; (b) Hexahedron; (c) Prism; (d) Tetrahedron; (e) Pyramid.

In order to show the capability of the EbFVM method to handle reservoir with irregular shapes, the next two case studies are related to an irregular reservoir. In both case studies, we have four producer wells near the borders of the reservoir, and two injector wells positioned next to central location of the reservoir. Figure 5 shows the two grid configurations used. For the second case study, we consider a fluid that contains three components. The pressure of the reservoir is high enough to maintain, initially, a single hydrocarbon phase. The injected fluid is rich in CO_2. The reservoir data and initial and injected fluid composition are presented in Tables 4 and 5, respectively.

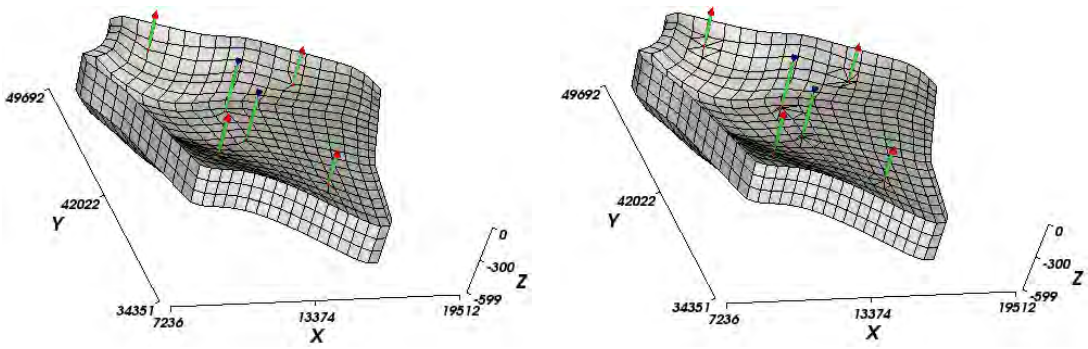

(a) (b)

Figure 4. Meshes for case studies 2 and 3. (a) Hexahedron grid with 1600 nodes; (b) Hybrid grid with 1744 nodes.

Table 4. Reservoir data for case 2.

Property	Value	Unit
Porosity	0.30	-
Water Initial Saturation	0.25	-
Initial Pressure	20.468	MPa
Permeability in X and Y	200	mD
Permeability in Z	20	mD
Formation Temperature	299.817	K
Producer Bottom Hole Pressure	20.468	MPa
Injector's Gas Rate	163.87	m^3/s

ISSN 2176-5480

Table 5. Fluid compositions for case 2.

Component	Initial Reservoir Composition	Injection Fluid Composition
CO_2	0.0100	0.9500
C1	0.1900	0.0500
C10	0.8000	0.0000

Figure 7 presents the oil and gas production rates. From this figure it possible to observe a good match between the results obtained with both grid configurations.

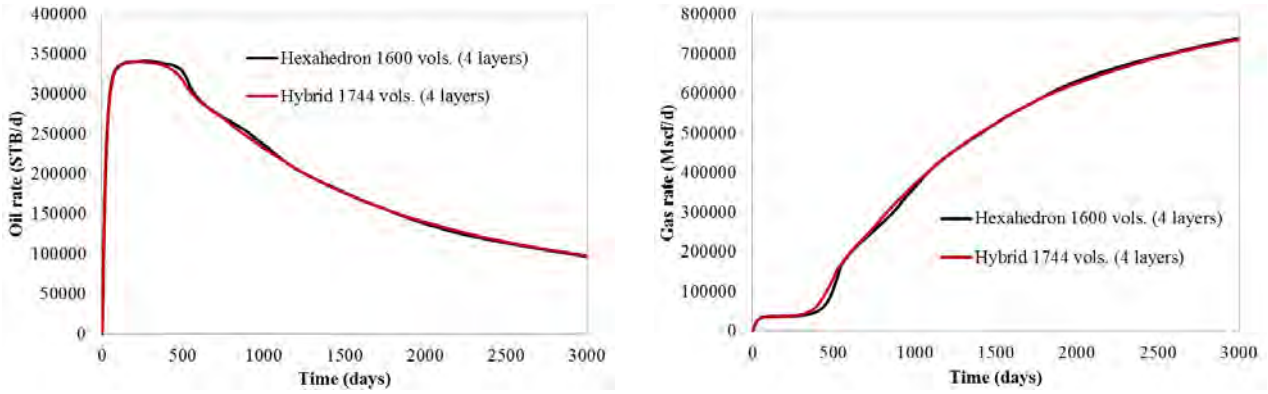

(a) (b)

Figure 4. Oil (a) and gas (b) rate for case 2.

Figure 5 presents the gas saturation field at 3000 days on the upper and bottom layer of the reservoir.

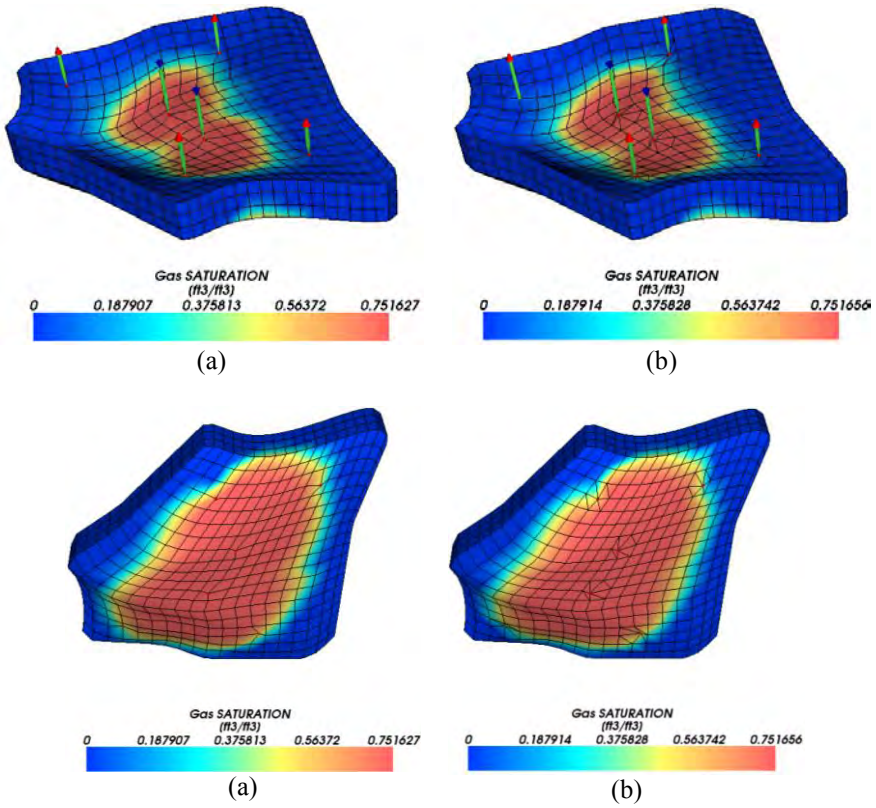

(a) (b)

(a) (b)

Figure 5. Gas saturation field at 3,000 days for case 2. a) Upper layer – hexahedron grid; b) Upper layer - hybrid grid; c) Bottom layer - hexahedron grid; (d) Bottom layer - hybrid grid.

ISSN 2176-5480

From Figure 5, it is possible to verify that the saturation field at upper and lower surface of the reservoir obtained with both grid configurations are in good match. The figure also shows the gas phase is flowing faster in the lower level of the reservoir. This behavior, at first look, seems to be incorrect. However, it is important to mention that the phase labeled as gas, is actually a supercritical phase rich in carbon dioxide. In this condition, the CO_2 rich phase has a higher density then the oil phase, and therefore it is will flow in deep region of the reservoir.

The last case study refers to a reservoir characterized by six hydrocarbon components. The reservoir is initially saturated. Tables 6 and 7 show the reservoir data set and fluid compositions, respectively.

Table 6. Reservoir data for case 3.

Property	Value	Unit
Porosity	0.35	-
Water Initial Saturation	0.25	-
Initial Pressure	10.340	MPa
Permeability in X and Y	10	mD
Permeability in Z	10	mD
Formation Temperature	344.26	K
Producer Bottom Hole Pressure	8.960	MPa
Injector's Gas Rate	4.916	m^3/s

Table 7. Fluid compositions for case 3.

Component	Initial Reservoir Composition	Injection Fluid Composition
C1	0.5000	0.7700
C3	0.0300	0.2000
C6	0.0700	0.0100
C10	0.2000	0.0100
C15	0.1500	0.0050
C20	0.0500	0.0050

The oil and gas rates are shown in Figure 6. From this figure, it is possible to verify again a good agreement between the curves obtained with both grid configurations.

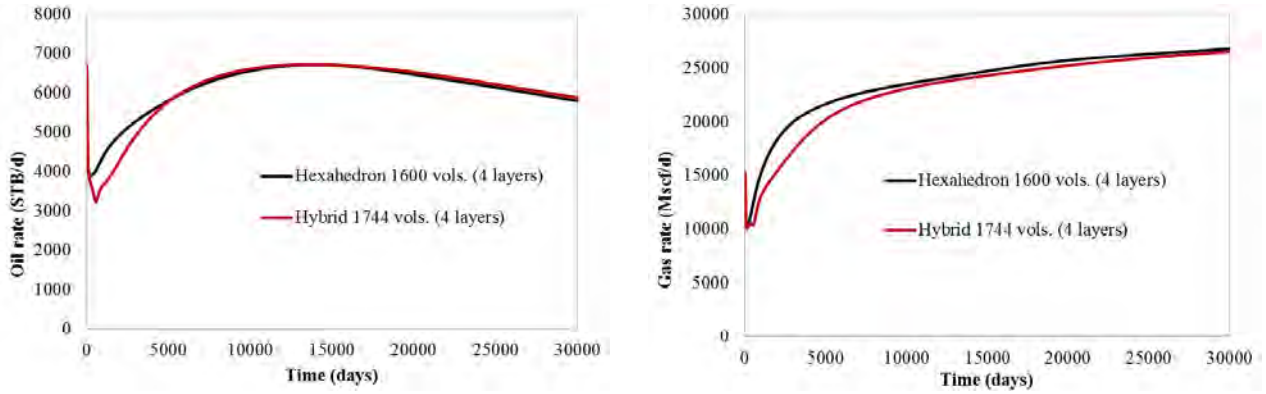

(a) (b)

Figure 6. Oil (a) and gas (b) rate for case 3.

The gas saturation fields at 3000 days for the upper and bottom level are shown below.

ISSN 2176-5480

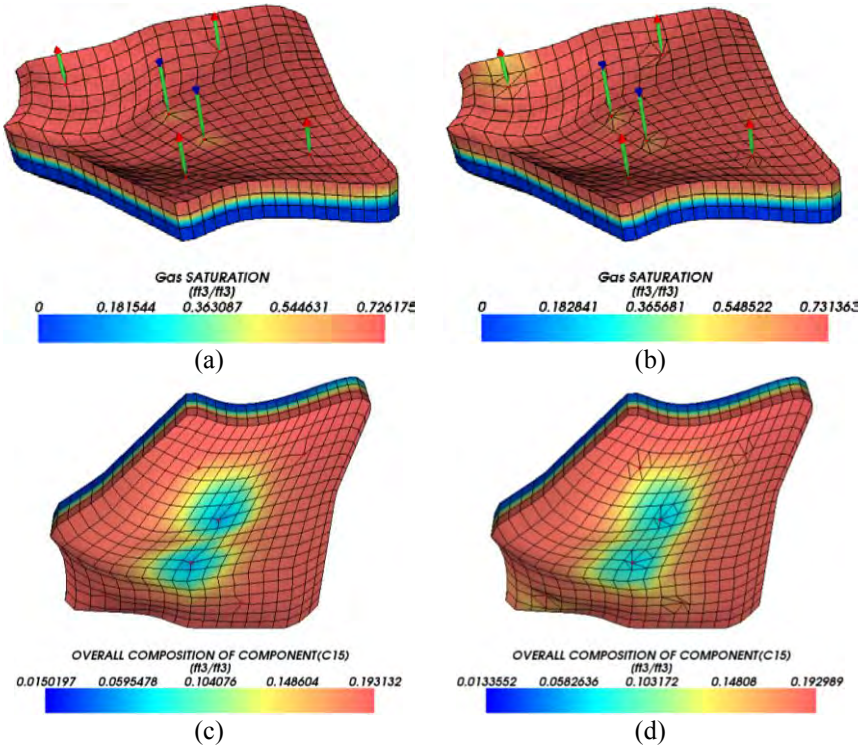

Figure 7. Gas saturation field at 3000 days for case 3. (a) Hexahedron grid, upper level; (b) Hybrid grid, upper level; (c) Hexahedron grid, bottom level; (d) Hybrid grid, bottom level.

In this conditions, it is impossible to make any conclusions bases only in the upper level fields, hence the importance of the bottom level fields, presenting the same tendency as the previous case. Also, the production rates show, again, a reasonable match.

5. CONCLUSION

This work presented an element-based finite volume method for 3D compositional reservoir simulations. The method was applied to hexahedron, tetrahedron, prism and pyramid element types for general geometries reservoirs. The results of the quarter of five-spot reservoir show a satisfactory accuracy for all four of elements, when compared among themselves, and, better yet, a good agreement with the Cartesian grid formulation. It is important to notice that these results were obtained with a much lower grid refinement then the Cartesian grid. The case studies also reveal the capacity to handle irregular reservoir geometries. This is shown by the good match between the hexahedron and the hybrid meshes. In conclusion, the EbFVM technique implemented was tested for various conditions and reservoirs, and, based on the presented results, the method shows great potential to solve problems with various geometries and special conditions, such as the formation of the carbon dioxide rich phase.

6. ACKNOWLEDGEMENTS

The authors would like to acknowledge the Petrobras S.A. for financial support. The support of the Center for Petroleum and Geosystems Engineering (CPGE) at The University of Texas at Austin for releasing the UTCOMP simulator to perform this work is also greatly appreciated.

7. REFERENCES

Baliga, B. R. and Patankar, S. V., 1983, A Control Volume Finite-Element Method for Two-Dimensional Fluid Flow and Heat Transfer, Numerical Heat Transfer, vol. 6, pp. 245-261.

Cordazzo, J., 2004, An Element Based Conservative Scheme using Unstructured Grids for Reservoir Simulation, SPE International Student Paper Contest, The SPE Annual Technical Conference and Exhibition, Houston, Texas.

Cordazzo, J., Maliska, C. R., Silva, A. F. C., and Hurtado, F. S. V., 2004, The Negative Transmissibility Issue When Using CVFEM in Petroleum Reservoir Simulation - 1. Theory", The 10th Brazilian Congress of Thermal Sciences and Engineering - ENCIT 2004, Braz. Soc. of Mechanical Sciences and Engineering - ABCM, Rio de Janeiro, Brazil, Nov. 29-Dec. 03.

ISSN 2176-5480

Cordazzo, J., Maliska, C. R., Silva, A. F. C., and Hurtado, F. S. V., 2004, The Negative Transmissibility Issue When Using CVFEM in Petroleum Reservoir Simulation - 2. Results, The 10th Brazilian Congress of Thermal Sciences and Engineering - ENCIT 2004, Braz. Soc. of Mechanical Sciences and Engineering - ABCM, Rio de Janeiro, Brazil, Nov. 29-Dec. 03.

Edwards, M. G., 2002, Unstructured, Control-volume Distributed, Full-Tensor Finite-Volume Schemes with Flow Based Grids, Computational Geosciences, vol. 6, pp. 433-452.

Forsyth, P .A. 1990, A Control-Volume, Finite-Element Method for Local Mesh Refinement in Thermal Reservoir Simulation, SPE paper 18415, (Nov.): pp. 561-566.

Fung, L. S., Hiebert, A. D. and Nghiem, L., 1991, Reservoir Simulation with a Control-Volume Finite-Element Method, Paper SPE 21224, The 11th SPE Symposium on Reservoir Simulation, Anaheim, California, February 17-20.

Gottardi, G. and Dall´Olio, D., 1992, A Control-Volume Finite-Element Model for Simulating Oil-Water Reservoirs, Journal of Petroleum Science and Engineering, vol. 8, pp. 29-41.

Hurtado, F. Finite Volume Tridimensional Formulation for Petroleum Reservoir Simulation with Unstructured Hybrid Grids. Ph.D. Dissertation, Federal University of Santa Catarina, Santa Catarina, Brazil, 2011. (In Portuguese)

Marcondes, F., Hang, C., and Sepehrnoori, K., 2008, Effect of Cross Derivatives in Discretization Schemes in Structured Non-Orthogonal Meshes for Compositional Reservoir Simulation, Journal of Petroleum Science & Engineering, 63, pp. 53-60.

Marcondes, F., and Sepehrnoori, K., 2007, Unstructured Grids and an Element Based Conservative Approach for Compositional Reservoir Simulation, The 19th International Congress of Mechanical Engineering, November 5-9, Brasília, DF, Brazil.

Marcondes, F., and Sepehrnoori, K., 2010, An Element-Based Finite-Volume Method Approach for Heterogeneous and Anisotropic Compositional Reservoir Simulation, Journal of Petroleum Science & Engineering, 73, pp. 99-106.

Marcondes, F., Santos, L., Varavei, A., and and Sepehrnoori, K., 2013, A 3D Hybrid Element-based Finite-volume Method for Heterogeneous and Anisotropic Compositional Reservoir Simulation, Journal of Petroleum Science & Engineering, 108, pp. 342-351.

Paluszny, A., Matthäi, and Hohmeyer, M., 2007, Hybrid Finite Element-Finite Volume Discretization of Complex Geologic Structures and a New Simulation Workflow Demonstrated on Fractured Rocks, Geofluids, 7, pp. 168-208.

Prévost, M., Edwards, M. G., and Blunt, M. J., 2002, Streamline Tracing on Curvilinear Structured and Unstructured Grids, SPEJ, vol. 7, pp. 139-148.

Raw, M., 1985, A New Control Volume Based Finite Element Procedure for the Numerical Solution of the Fluid Flow and Scalar Transport Equations, Ph.D. Thesis, University of Waterloo, Waterloo, Ontario, Canada.

Wang, P., Yotov, I., Wheeler, M., Arbogast, T., Dawson, C., Parashar, M., and Sepehrnoori, K., 1997, A New Generation EOS Compositional Reservoir Simulator: Part I – Formulation and Discretization, Paper SPE 37079, SPE Reservoir Simulation Symposium, Dallas, Texas.

8. RESPONSIBILITY NOTICE

The authors are the only responsibles for the printed material included in this paper.